Treatment Potential for Macular Cone Vision in Leber Congenital Amaurosis Due to *CEP290* or *NPHP5* Mutations: Predictions From Artificial Intelligence

Alexander Sumaroka, Alexandra V. Garafalo, Evelyn P. Semenov, Rebecca Sheplock, Arun K. Krishnan, Alejandro J. Roman, Samuel G. Jacobson, and Artur V. Cideciyan

Scheie Eye Institute, Department of Ophthalmology, Perelman School of Medicine, University of Pennsylvania, Philadelphia, Pennsylvania, United States

Correspondence: Artur V. Cideciyan, Scheie Eye Institute, University of Pennsylvania, 51 North 39th Street, Philadelphia, PA 19104, USA; cideciya@pennmedicine.upenn.edu. Samuel G. Jacobson, Scheie Eye Institute, University of Pennsylvania, 51 North 39th Street, Philadelphia, PA 19104, USA; jacobsos@pennmedicine.upenn.edu.

Submitted: March 23, 2019
Accepted: May 19, 2019

Citation: Sumaroka A, Garafalo AV, Semenov EP, et al. Treatment potential for macular cone vision in Leber congenital amaurosis due to *CEP290* or *NPHP5* mutations: predictions from artificial intelligence. *Invest Ophthalmol Vis Sci*. 2019;60:2551–2562. https://doi.org/10.1167/iovs.19-27156

Purpose. To use supervised machine learning to predict visual function from retinal structure in retinitis pigmentosa (RP) and apply these estimates to *CEP290*- and *NPHP5*-associated Leber congenital amaurosis (LCA) to determine the potential for functional improvement.

Methods. Patients with RP ($n = 20$) and LCA due to *CEP290* ($n = 12$) or *NPHP5* ($n = 6$) mutations were studied. A patient with *CEP290* mutations but mild retinal degeneration was included. RP patients had cone-mediated macular function. A machine learning technique was used to associate perimetric sensitivities to local structure in RP patients. Models trained on RP data were applied to predict visual function in LCA.

Results. The RP and LCA patients had comparable retinal structure. RP patients had peak sensitivity at the fovea surrounded by decreasing sensitivity. Machine learning could successfully predict perimetry results from segmented or unsegmented optical coherence tomography (OCT) input. Application of machine learning predictions to LCA within the residual macular island of photoreceptor structure showed differences between predicted and measured sensitivities defining treatment potential. In patients with retained vision, the treatment potential was 4.6 ± 2.9 dB at the fovea but 16.4 ± 4.4 dB at the parafovea. In patients with limited or no vision, the treatment potential was 17.6 ± 9.4 dB.

Conclusions. Cone vision improvement potential in LCA due to *CEP290* or *NPHP5* mutations is predictable from retinal structure using a machine learning approach. This should allow individual prediction of the maximal efficacy in clinical trials and guide decisions about dosing. Similar strategies can be used in other retinal degenerations to estimate the extent and location of treatment potential.

Keywords: machine learning, random forest, optical coherence tomography, chromatic perimetry, retinal degeneration, rods, cones

The field of inherited retinal degenerations (IRDs) is emerging from its long history when the diseases were considered as incurable to the current time when there are potential therapies. The ultimate goal of all such treatment is to improve vision that has either been progressively lost or was very limited or never useful from early life. Once safety of the product is established in early phase trials, reckoning with efficacy needs to occur. Ideally, efficacy may occur posttreatment in the form of dramatic visual improvement but an alternative outcome, which is also welcomed by most patients with progressive loss of vision, is a slowing of the relentless degenerative process. Contributing to the complexity of determining outcome is whether there is sufficient knowledge about the human disease mechanism (by in vitro or disease model research), the stages of the human disease, and which noninvasive outcomes are best to use to decipher what effects the product is having on the retina.[1,2]

It is of historic interest that in 1983, a group of experts at a specialty symposium declared that no specific therapy existed for RP.[3] Now, after more than 3 decades, we have one therapy for one disease and this IRD, which showed improvement in vision after gene augmentation but later lost some of it to degeneration,[4,5] is in the family of disorders known as Leber congenital amaurosis (LCA). The human studies of this *RPE65* form of LCA determined that a key finding was the dissociation of function and structure.[6] This finding allowed for hope that if the visual cycle pathway was restored by *RPE65* gene augmentation to a patch of RPE cells, then adjacent dysfunctional photoreceptors may respond to the renewed source of vitamin A as occurred in canine and rodent models of the disease.[7–9]

Two other forms of LCA, those due to mutations in *NPHP5* and *CEP290*, are primary photoreceptor diseases rather than RPE diseases, and the molecules are reported to form a complex in the cilium.[10–13] Of strong interest to those seeking therapies for LCA, these two early-onset seriously visually disabling disorders show very similar phenotypes and there is dissociation of structure and function.[14–19] As clinical trials in these disorders proceed[20] or are being planned,[21] there have been no attempts to predict the best visual outcome possible from the retinal structure retained at the time of the intervention.

Machine learning techniques have been used to diagnose certain ocular diseases and monitor progression with the

Table 1. Clinical Characteristics of RP Patients Used in Training Random Forest Algorithm

Patient	Sex	Age at Exam	Best-Corrected Visual Acuity*	Refractive Error†	Gene
P1	M	18	20/25 (+0.1)	−0.50	*RPGR* ORF15
P2	F	21	20/20 (0.0)	−2.50	unk.
P3‡	M	21	20/32 (+0.22)	−1.75	*WDR19*
P4‡	M	21	20/32 (+0.22)	+1.50	*WDR19*
P5	M	26	20/32 (+0.22)	−4.50	*RPGR* ORF15
P6	M	32	20/25 (+0.1)	−1.00	*RPGR*
P7	F	35	20/20 (0.0)	−0.25	unk.
P8	M	36	20/32 (+0.22)	−12.50	*USH2A*
P9	M	38	20/20 (0.0)	−3.75	*RHO*
P10	F	39	20/40 (+0.3)	−0.50	*DHDDS*
P11	F	40	20/32 (+0.22)	−0.25	unk.
P12	F	41	20/32 (+0.22)	+0.50	unk.
P13	M	41	20/25 (+0.1)	+0.25	*USH2A*
P14	F	48	20/25 (+0.1)	−5.00	unk.
P15	F	48	20/25 (+0.1)	−2.25	*RHO*
P16	M	53	20/25 (+0.1)	−1.25	*RHO*
P17	M	54	20/40 (+0.3)	−0.75	*USH2A*
P18	M	55	20/20 (0.0)	−1.25	*MAK*
P19	M	56	20/32 (+0.22)	−1.25	*USH2A*
P20	F	58	20/32 (+0.22)	−5.75	*MAK*

unk., gene causing disease is unknown; *RPGR* (*ORF 15*), retinitis pigmentosa GTPase regulator (open reading frame 15); *WDR19*, WD repeat domain 19; *USH2A*, Usherin; *RHO*, rhodopsin; *DHDDS*, dehydrodolichyl diphosphate synthase subunit; *MAK*, male germ cell-associated kinase.

* Visual acuity for eye with OCT used in training given in Snellen (and logMAR).

† Spherical equivalent for eye with OCT used in training.

‡ Patients are siblings.

ultimate goal of early detection and treatment.[22–24] In the present work, we used these methods to try to predict from cross-sectional retinal structure images with optical coherence tomography (OCT) what would be the best possible visual outcome in a clinical trial of these previously incurable forms of *CEP290*- or *NPHP5*-associated LCA.

Methods

Human Subjects

Data from patients with RP ($n = 20$, aged 18–58, Table 1) with retained cone-mediated sensitivities, retained visual acuities (better than 20/40), and retained foveal outer photoreceptor nuclear layer (ONL) thickness (>35 μm but <140 μm) were included in this study. Patients with cystoid macular edema (CME) were excluded. In addition, there were 18 patients with the clinical diagnosis of LCA and mutations in the *CEP290* or *NPHP5* genes (Table 2). All *CEP290* patients were non-syndromic LCA with no other organ system involvement. All *NPHP5* patients were syndromic with kidney disease (nephronophthisis) but will be referred to as LCA for simplicity due to the similarity of the retinal disease between the two genotypes. A 26-year-old patient with two *CEP290* mutant alleles and a relatively mild retinal degeneration was also included. All subjects underwent a complete eye examination as well as specialized tests of visual function and structure. Data from one eye were included for each patient. The research was approved by the institutional review board at the University of Pennsylvania. All subjects were treated in accordance with the tenets of the Declaration of Helsinki, and informed consents were obtained from all patients.

Table 2. Clinical Characteristics of *NPHP5* and *CEP290* Patients

Gene - Phenotype	Patient	Sex	Age at Exam	Best-Corrected Visual Acuity*	Refractive Error†
CEP290 - LCA	P21	F	12	20/80 (+0.6)	+2.75
	P22	F	13	NLP	+3.25‡
	P23	F	14	LP	+11.00
	P24	F	16	LP	+1.75
	P25	F	17	LP	+8.00‡
	P26	M	18	BLP	+7.00‡
	P27	M	19	NLP	+11.00
	P28§	F	19	20/50 (+0.4)	+4.75
	P29§	M	27	LP	+4.50
	P30	F	28	20/250 (+1.1)	+5.00
	P31	F	29	LP	+9.50
	P32	F	30	20/50 (+0.4)	+5.50
CEP290 - RD	P33	M	26	20/20 (0.0)	−8.50
NPHP5 - LCA	P34	M	7	20/400 (+1.3)	+6.00
	P35#	M	12	LP	+7.50
	P36	M	13	20/200 (+1.0)	+4.00
	P37#	M	15	LP	+9.00
	P38	F	18	20/100 (+0.7)	−2.00
	P39	F	23	20/80 (+0.6)	+1.00

LCA, leber congenital amaurosis; RD, retinal degeneration.

* Visual acuity for eye with OCT used in analysis given in Snellen (and logMAR).

† Spherical equivalent for eye with OCT used in analysis.

‡ Refractive error was not measured at this visit but was from a previous visit.

§ Patients are siblings.

Patients are siblings.

Optical Coherence Tomography (OCT)

Retinal cross-sections along the horizontal meridian crossing the fovea were obtained with OCT (RTVue-100; Optovue Inc., Fremont, CA, USA) in all patients but one (P28), which was scanned with time-domain OCT (OCT3; Carl Zeiss Meditec, Dublin, CA, USA). The principles of the method and our recording and analysis techniques have been published.[15,25–27] Postacquisition processing of OCT data was performed with custom programs (MATLAB 2018a; MathWorks, Natick, MA, USA). All scans were preprocessed by aligning the longitudinal reflectivity profiles (LRPs) making up the OCT scans by manually defining the depth of the highly hyperreflective signal believed to originate near the interface of basal RPE and Bruch membrane (BrM). The foveola was identified manually as the maximum depression. For the supervised learning algorithm requiring segmented OCT layers as input features, the following layer boundaries were defined manually with a computer assisted algorithm. The ONL was defined as the major intraretinal signal trough delimited by the outer plexiform layer (OPL) and external limiting membrane (ELM) as previously described.[28] Inner retina was defined between inner limiting membrane and the vitreal boundary of OPL. Inner and outer segment (IS+OS) layer was defined between ELM and the inner boundary of RPE, and the RPE layer between inner boundary of the RPE and BrM. In addition, the number of negative and positive peaks (extrema) on the gradient of the LRPs inside the IS+OS layer was automatically counted.

Chromatic Dark-Adapted Static Perimetry

Dark-adapted static perimetry (Humphrey Field Analyzer, HFA-750i analyzer; Zeiss-Humphrey, Dublin, CA, USA) was performed[25,29] along the horizontal meridian in all RP

patients and a subset of the LCA patients who retained sufficient fixation. Testing was with two colors (500 nm, blue; 650 nm, red) using 1.7° diameter, 200-ms duration stimuli sampling the visual field at 2° intervals. The perimetric results when available will be referred to as B-HFA and R-HFA. The blue minus red differences in all RP patients showed cone mediation (≤12 dB) at all tested locations as a requirement for inclusion. For the red stimulus, 0 dB corresponded to a luminance of 12 phot-cd.m^{-2}. Normal dark-adapted cone sensitivities were from the cone-plateau region for red as previously published[25] or extrapolated from red to blue using standard chromatic sensitivity differences.

Full-Field Sensitivity Testing (FST)

In the majority of LCA patients without fixation, FST sensitivities were measured with blue (B-) and red (R-) full-field stimuli (200-ms duration) in the dark-adapted state.[30,31] FST results represent the retinal locus with the highest sensitivity.[30] FST sensitivities were converted to HFA sensitivity scales and assigned to the foveal locus under the assumption of the fovea being the most sensitive locus with cone function in *CEP290*- and *NPHP5*-LCA. The FST results will be referred to as B-FST and R-FST.

Data Analysis

A supervised machine learning approach was taken to model the relationship between localized retinal function and localized retinal structure in RP patients and apply the model to predict locus-by-locus treatment potential in *CEP290*- and *NPHP5*-LCA. An implementation (MATLAB 2018a; MathWorks) of the random forest regression model[32] was setup with and trained on RP patient data using input features derived from OCT scans and target variables derived from chromatic dark-adapted sensitivities. Four separate but similar models were constructed based on two forms of input features and two forms of target variables (Supplementary Fig. S1). For Model I, the following measured input features were sampled at 2° intervals: inner retina thickness, ONL thickness, IS+OS layer thickness, RPE thickness, and the number of distinct layers within IS+OS. Additionally, the relationship between input features (thickness of all layers, except for the RPE, which did not substantially vary with eccentricity) and retinal eccentricity were accounted for by directly including interaction terms, which yielded a total of 10 input variables (Supplementary Fig. S1B). For Model II, there was no segmentation of layers. Instead, reflectivity values at each depth with respect to the RPE/BrM were the input features with a multiresolution approach using three resolutions of depth binning at each locus. Similar to Model I, the product of retinal eccentricity with each reflectivity value (for scales 2 and 3), and eccentricity alone were used as input features as well (Supplementary Fig. S1C). A total of 91 predictors were included in Model II. For Model R, red sensitivity values were used as the target variable and for Model B, blue sensitivity values were used as the target variable. The combination of input and target variables corresponded to four distinct models, which will be referred to as Models I-R, I-B, II-R, and II-B (Supplementary Figs. S1D, S1E).

Performance of each model was evaluated by leave-one-out, 20-fold cross-validation; the error between the measured target variable (sensitivity) and the predicted value, based on the remaining 19 patients, was calculated. Errors across all patients were summarized by calculating the 95th percentile limits of agreement (LoA).[33] Final models were trained using data from all 20 RP patients, and relative importance of the individual input features was evaluated automatically, as part of the Matlab algorithm implementation, by measuring any decrease in prediction accuracy from permuting the values of each input variable.

Results

Retinal Structure With Only Cone Photoreceptors Remaining

Previous studies have demonstrated that the great majority of patients with *CEP290*- or *NPHP5*-LCA share a stereotypical retinal structure.[14–16,18–20,34–36] Specifically, there is a macular elliptical region of approximately 13° width and 10° height by en face near-infrared imaging.[14,19] Within this area, by OCT, are relatively healthy appearing photoreceptors surrounded by severe photoreceptor loss in the extracentral retina. At the fovea, photoreceptor ONL thickness is normal or near-normal and there is increasingly abnormal thinning as a function of distance from the fovea (Fig. 1A). Beyond 5° to 8° in eccentricity, ONL either asymptotes to a thin layer or is not detectable. Considerable clinical and preclinical data support the hypothesis that the mound of retained photoreceptors in *CEP290*- or *NPHP5*-LCA are cone photoreceptors.[14–16,18–20,34,35]

RP is a genetically heterogenous condition with a variety of phenotypes and genotypes.[37–39] Independent of the exact genetic cause, a relatively common later stage of RP involves a central macular region of visual function mediated only by cone photoreceptors (Pattern 3[25]; Ref. 40). We selected a cohort of 20 such RP patients (Table 1); they all had a central mound of ONL thickness resembling the retinal structure of *CEP290*- or *NPHP5*-LCA patients (Fig. 1A). Foveal ONL thickness ranged from normal to mildly thinned, and overlapped with the LCA patients. Width of retained ONL ranged from 12.5° to 18° and overlapped with the LCA patients (Fig. 1B). The overall aim was to compare the localized visual function between RP and LCA patients when matched by structure.

Machine Learning to Predict Local Function From Local Structure in RP

As a first step, we asked whether a machine learning algorithm can be trained to predict reliably the local variation in cone sensitivity based on co-localized variation in retinal structure in RP. We used a random forest supervised learning algorithm with the local structure parameters as input and red or blue dark-adapted sensitivities as output and built four distinct models (Supplementary Fig. S1). For each of the models based on scan segmentation (Models I-R and I-B) the total number of input features was 1800 (9 loci × 20 patients × 10 features per locus). For each of the models based on multiscale reflectivity (Models II-R and II-B), the total number of input features was 16,380 (9 loci × 20 patients × 91 features per locus). Total number of target variables for each model was 180 (9 loci × 20 patients). Measured and predicted sensitivities were compared locus by locus for all RP patients and all models using leave-one-out cross-validation. Four RP patients illustrate the range of results obtained over a spectrum of disease severities (Fig. 2). P15 and P20 exemplify milder central retinal disease with normal or near-normal sensitivities at the fovea and retained IS/OS structure, whereas P17 and P10 exemplify more severe disease with greater foveal abnormalities in function and structure. The predictions of the four models appear to approximate well the measured visual sensitivity values (Fig. 2).

Investigative Ophthalmology & Visual Science

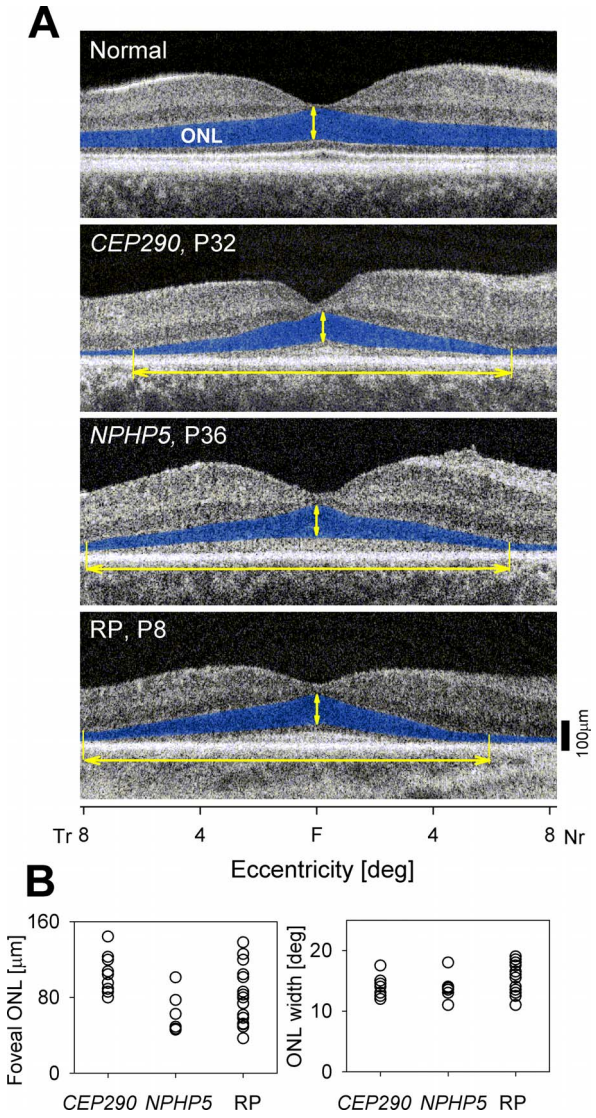

Figure 1. Comparison of retinal structure between LCA patients with *CEP290 or NPHP5* mutations and RP patients with cone-mediated macular function. (**A**) OCT scans along the horizontal meridian crossing the fovea in a normal subject and representative patients. ONL is highlighted in *blue* for visibility; *yellow vertical arrows* show the foveal ONL thickness; *yellow horizontal arrows* show the width of retained ONL in each image. (**B**) Plots comparing foveal ONL thickness and width of retained ONL for *CEP290*-LCA, *NPHP5*-LCA and RP patients; *open circles* are measurements for each patient studied. F, fovea; Tr, temporal retina; Nr, nasal retina.

Across all RP patients, point-by-point differences between measured and predicted sensitivities were compared using a mixed-effects model to account for the internal correlation structure of the data. For red stimuli using the segmented OCTs (Model I-R), LoA was 9.6 dB, and for blue stimuli using segmented OCTs (Model I-B), LoA was 8.8 dB (Fig. 3A). The point-by-point differences were similar to the 9.6 dB coefficient of repeatability estimated from test-retest differences using dark-adapted blue sensitivities.[41] Including a linear trend component to account for a relation between the difference and average did not produce a significantly better quality of fit to the data than a simpler model without this trend ($P = 0.0911$ and 0.5 for I-R and I-B, respectively). The biases of the simpler model were not significantly different than zero ($P = 0.397$ and 0.266 for I-R and I-B, respectively).

Similar analyses with unsegmented OCT input based on multiscale reflectivity values, the 95% LoA were 11.9 and 10.8 dB for red and blue stimuli, respectively (Fig. 3B). Including a linear trend component to account for a relation between the difference and average did not produce a significantly better quality of fit to the data than a simpler model without this trend ($P = 0.0904$ and 0.224 for II-R and II-B, respectively). The biases of the simpler model were not different than zero ($P = 0.618$ and 0.3 for II-R and II-B, respectively).

Comparability of the Segmented and Unsegmented Retinal Structure Inputs

Predictions of visual function from segmented retinal structure input (Model I) were highly similar to the predictions from unsegmented input for red (Supplementary Fig. S2A) and blue (Supplementary Fig. S2B) stimuli (LoA red models = 6.57 dB, LoA blue models = 5.2 dB, no significant bias in either comparison). To better understand the contributions of different features used by the machine learning algorithms, we evaluated their relative importance. For Model I-R using segmented OCT layer thicknesses, features of greatest importance were IS+OS and ONL thickness (Supplementary Fig. S3A). RPE thickness, was least important for prediction of red and blue sensitivities. Feature importance for Model I-B was similar. For Model II-R using unsegmented LRP intensity information, the features of greatest importance were located at 15 to 50 µm vitreal to the BrM at all three scales (Scale 2 shown, Supplementary Fig. S3B). This location would be expected to correspond to inner and outer segments. In terms of the interaction of eccentricity and reflectivity, two peaks of feature importance were located 0 to 40 µm choroidal and 70 to 120 µm vitreal to the BrM (Scale 2 shown, Supplementary Fig. S3B). These locations would be expected to correspond to choroid and ONL, respectively. Not unexpectedly, all four models were using mostly information content originating at or near the photoreceptor layer to predict photoreceptor function.

Predicted and Measured Sensitivities in *CEP290*-LCA

We first tested our predictions of locus-by-locus sensitivity in a patient with *CEP90* mutations causing retinopathy that was much milder in disease expression than in LCA; the model predictions corresponded closely to the perimetric macular visual function measured in this patient (P33, Fig. 4). In the cohort of LCA patients, however, it was rare to have measured sensitivities that were similar to predicted sensitivities at most locations. In the group of four patients with measurable acuity and sufficient fixation to perform the dark-adapted perimetric profiles, only one came close to approximating measured function to the function predicted from the models (P28, Fig. 4). The other three patients (P32, P21, and P30) had expected function at the foveal locus only. Most paracentral loci that were predicted to have visual function based on structure were not visually responsive.

Of the 12 patients with *CEP290*-LCA studied, eight had clinically measured light perception (LP) or no light perception (NLP); in these patients, chromatic FSTs were performed (Fig. 5). Previous experimental evidence has indicated that FST results emanate from the most sensitive locus in the retina of the patient[30] and in the case of these *CEP290*-LCA patients, the most sensitive locus was assumed to be at the fovea corresponding to the peak ONL thickness. This assumption was consistent with the peaky shape of sensitivity profiles in the subset of patients (Fig. 4). One patient with LP (who had retained 2.6 logMAR acuity when tested with low vision specific methods) had normal FST sensitivity for cone-mediated

Investigative Ophthalmology & Visual Science

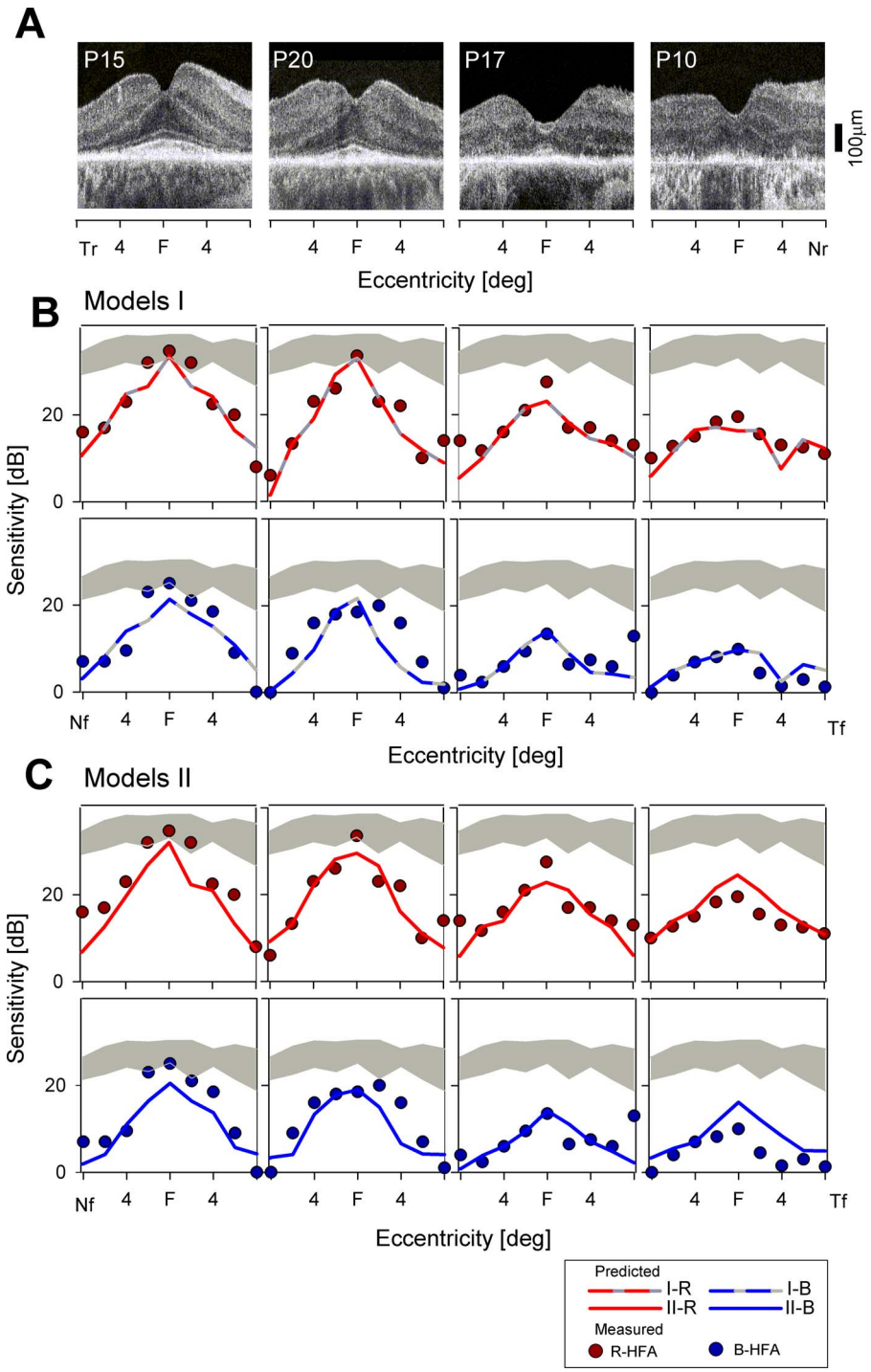

Figure 2. Comparison of measured perimetric sensitivities with predicted sensitivities for RP patients, as derived from the leave-one-out cross-validation of the random forest–based models. (**A**) OCTs of four representative RP patients used in training, taken along the horizontal meridian, crossing the fovea. Two are less severely affected (P15, P20), while two are more severely affected (P17, P10). (**B**) For each patient, plots show the comparison of predicted sensitivities from Model I-R (*upper panels*) and Model I-B (*lower panels*) to measured perimetric sensitivities. (**C**) Predicted perimetric sensitivities from Model II-R and Model II-B are compared with measured perimetric sensitivities. (**B**, **C**) *Red circles* denote measured red dark-adapted perimetry (R-HFA) sensitivities; *blue circles* denote blue dark-adapted (B-HFA) perimetry results; mean Model I predictions of sensitivity are given as *dashed lines*; mean Model II predictions are given as *solid lines. Gray shaded areas* represent the bounds for normal dark-adapted cone sensitivities. Nf, nasal field (corresponding to temporal retina); Tf, temporal field (corresponding to nasal retina).

function and this matched the expectation of the models at the fovea (P24, Fig. 5). Although the reason for the lack of better visual acuity in this patient remains unknown, it was clear from visual behavior during OCT testing that unlike the other LP-vision patients, there was the ability to fixate at the fovea. The remaining seven patients had no fixation and limited or no measurable sensitivity to FST stimuli and showed a major mismatch between predicted and measured function (Fig. 5).

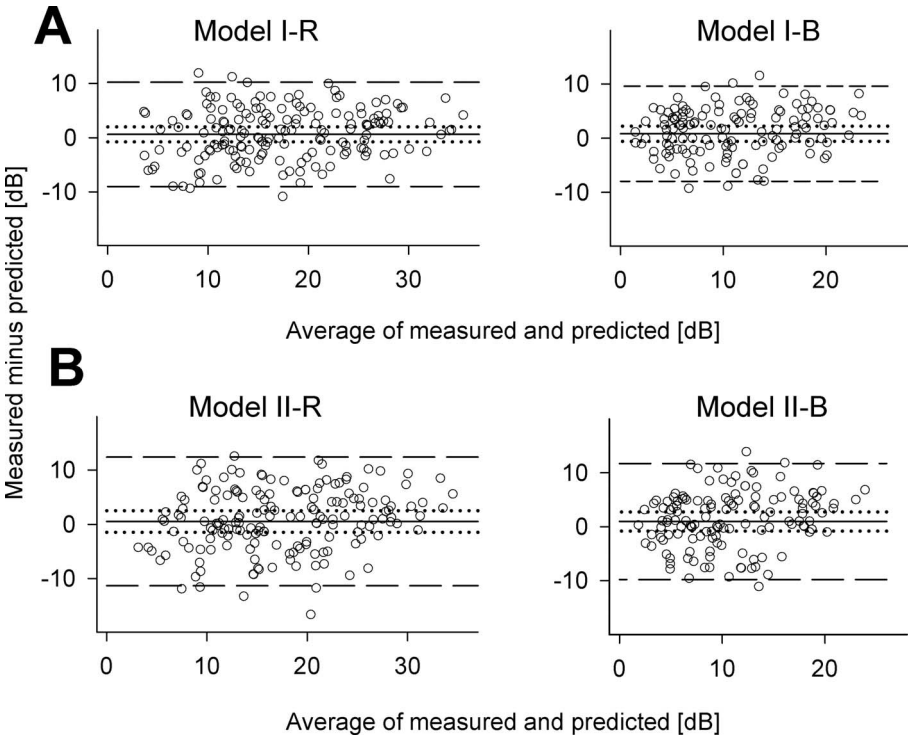

FIGURE 3. Bland-Altman plots show the LoA of the supervised learning models in predicting cone sensitivities from retinal structure in RP patients. The 95% LoA are given as the *dashed lines*. Mean bias values and their 95% CI are shown with *solid and dotted lines*, respectively. (**A**) Bland-Altman plot for Model I. (**B**) Bland-Altman plot for Model II.

Predicted and Measured Sensitivities in *NPHP5*-LCA

NPHP5-LCA patients also showed a range of functional phenotypes with the same patterns as in *CEP90*-LCA. Three patients with retained acuity and foveal fixation (P39, P38, and P36, Fig. 6) showed foveal sensitivities that were within approximately 5 dB of the value predicted by models. Paracentral loci were either unresponsive or greatly diminished in sensitivity compared with the expectation from retinal structure. One patient (P34, Fig. 6) had retained FST sensitivity that matched the prediction by models at the fovea. Two patients with LP vision and no ability to fixate (P35, P37, Fig. 6) had measurable FST results but there were large differences from sensitivity predictions of the models.

Treatment Potential in *CEP290*-LCA and *NPHP5*-LCA

Previous investigations have supported the hypothesis that *CEP290*- and *NPHP5*-LCA patients tend to show dissociation of function from structure.[14–16,18,19,34,36] Consistent with this hypothesis were preliminary results showing sensitivity improvements in a clinical trial involving antisense gene therapy in *CEP290*-LCA.[20] However, quantitative estimates of the maximal treatment potential at specific retinal loci of individual *CEP290*- or *NPHP5*-LCA patients were not known until the current work.

The differences between measured and predicted sensitivities (Figs. 4–6) provide the extent of maximal treatment potential. A subset of seven patients with relatively preserved acuity, fixation, and ability to perform perimetric testing have retained foveal sensitivity and thus relatively small treatment potential (4.6 ± 2.9 dB for red, 5.0 ± 3.5 dB for blue) at the fovea (Fig. 7A, left). The majority of the remaining 11 patients with unmeasurable acuity, lack of fixation and reduced sensitivity have large treatment potential (17.6 ± 9.4 dB for red, 12.5 ± 4.0 dB for blue, Fig. 7A, right). Unknown and unpredictable until the current work was the treatment potential in the paracentral retina of patients with retained foveal vision (Fig. 7B). The difference between measured and predicted sensitivities peak at 2° eccentricity in the parafovea where the maximal treatment potential reaches 16.4 ± 4.4 dB for red and 8.8 ± 2.8 dB for blue stimuli. At greater eccentricities, the treatment potential is gradually reduced as retinal locations reach the edge of the retained ONL region (Fig. 7B).

DISCUSSION

Using Later Stage RP Data to Understand LCA

In the modern retina clinic, OCT is frequently used in evaluations of patients with RP. A retina clinician viewing a scan that is recorded through the fovea in RP patients at certain disease stages often notices that instead of the ONL extending across the entire central scan there is a triangular shape to the ONL. From a peak at the fovea, there can be a decrease of ONL thickness with eccentricity. Given greater resolution of OCT instrumentation and many studies of the relationship of OCT sublaminae to retinal microstructure, attention has also been drawn to the other hyper- and hyporeflective structures deep to the ONL (e.g., see Refs. 42–44). When results of static perimetry are known in such RP patients, it becomes understandable that the central island of vision is likely related to this triangle of photoreceptor structure (e.g., see Refs. 45, 46).

In the present work, we carefully selected RP patients who were at a disease stage with only functional cone photoreceptors remaining in the macula.[25] We assumed lack of rod

Investigative Ophthalmology & Visual Science

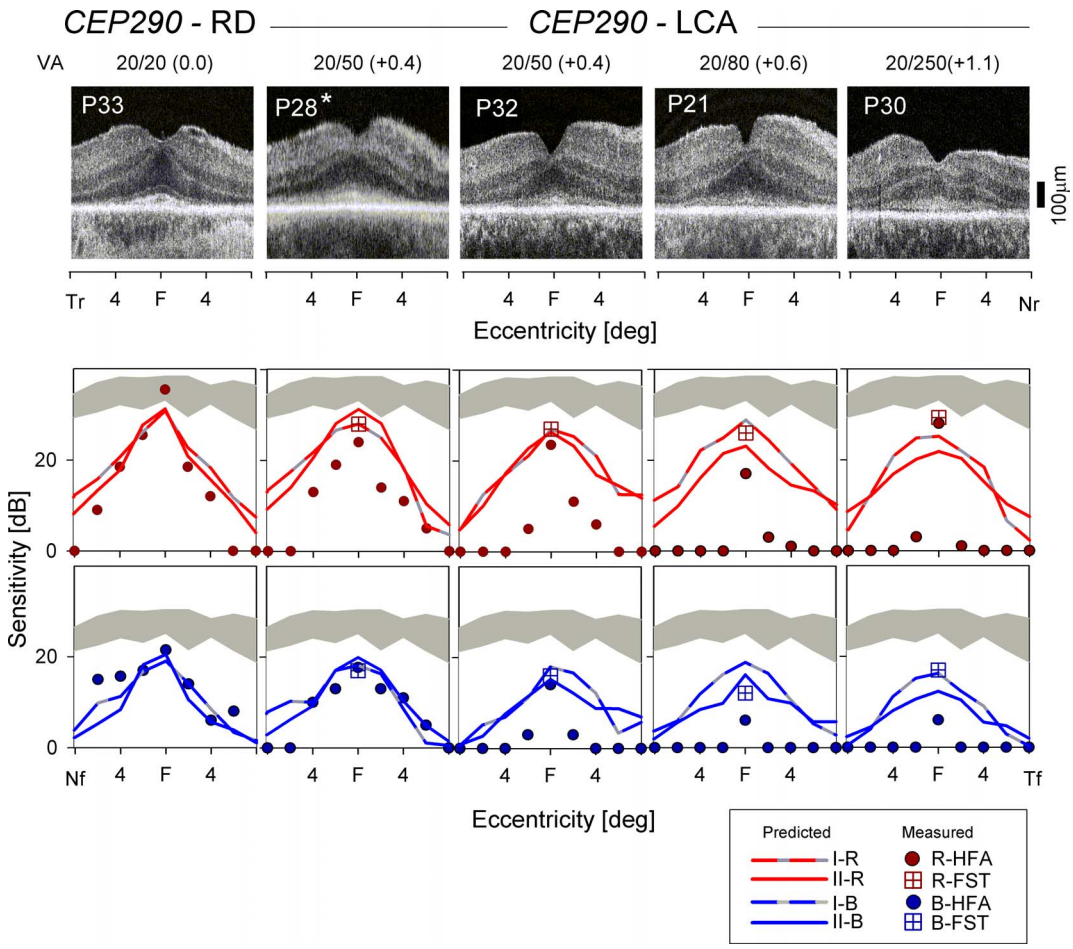

Figure 4. Predicted and measured perimetric sensitivities for a subset of *CEP290* patients with retained acuities and fixation. The *upper row* shows OCT scans taken along the horizontal meridian, crossing the fovea. Visual acuities (VA) are given above each patient scan in Snellen (logMar). P33 was diagnosed as having a milder inherited retinal degeneration (*CEP290*-RD) and not LCA, as in all other patients with *CEP290* mutations. The *middle row* compares the measured perimetric sensitivities with red stimuli (R-HFA) with the sensitivities predicted from the OCT scans using Model I-R and Model II-R; the *lower row* compares the measured and predicted results with blue stimuli. The *asterisk* for P28 denotes that the OCT image used to predict function was an OCT3 scan rather than an Optovue scan. Prior to analysis, the OCT3 image was resampled and the values were transformed so image size and histogram matched that of an Optovue scan.

photoreceptors based on severe lack of rod function. We assumed that the cones in this cohort of RP patients were functioning proportional to their remaining quantum catch and there was no additional de-sensitization beyond the partial loss of cones and shortening of OS among the surviving cones. Support for the lack of additional de-sensitization mechanisms in the selected RP eyes came from normal thresholds in eight of the patients at the fovea. For the retinal locations with losses of sensitivity the validity of our assumption is consistent with some of the previous work on comparable patients at the fovea[6,18,47,48]; however, extrafoveal structure–function relationships cannot be confirmed at this time.

Molecular classification of LCA has led to the study of the disease expression in different subtypes and it became obvious that the CEP290 and NPHP5 forms of LCA also showed a triangular shape to the central ONL.[14–19] The notable difference between these LCA patients and the RP patients was that in LCA, there was more severe dysfunction within the central island. The concept of dissociation of structure and function was proposed, and the present work has attempted to extend this hypothesis by predicting the exact degree of this dissociation across the central retina and thus defining the maximal treatment potential with future optimal therapies.

Predicting Efficacy Outcomes With Machine Learning in This Era of LCA Therapy

Although use of machine learning in medical research, and particularly in ophthalmology, has exploded in recent years,[24,49] the great majority of the published work to date is in the fields of diagnostics[50–53] and image segmentation.[54,55] Other groups have used machine learning to predict measures of visual function from multiple input parameters, such as predicting visual acuity in AMD based on a variety of inputs, including retinal structure[56] or predicting static perimetry sensitivities in glaucoma, based on previous such results and clinical parameters.[57] Recently, neural networks were used for the first time to predict local function (microperimetric sensitivity) from retinal structure in patients with macular telangiectasia.[58] In the present study, we extended the function-from-structure concept one step further. We used random forest algorithms trained on OCT scans from one retinal disease, that of RP with cone-only central islands, to predict retinal function in two genetic types of LCA, which are characterized by similar retinal structure.

What is the current process for gene-based clinical trials from defining patient eligibility to evaluation of a product's efficacy? Eligibility requires a clinical diagnosis and, of course, a

Investigative Ophthalmology & Visual Science

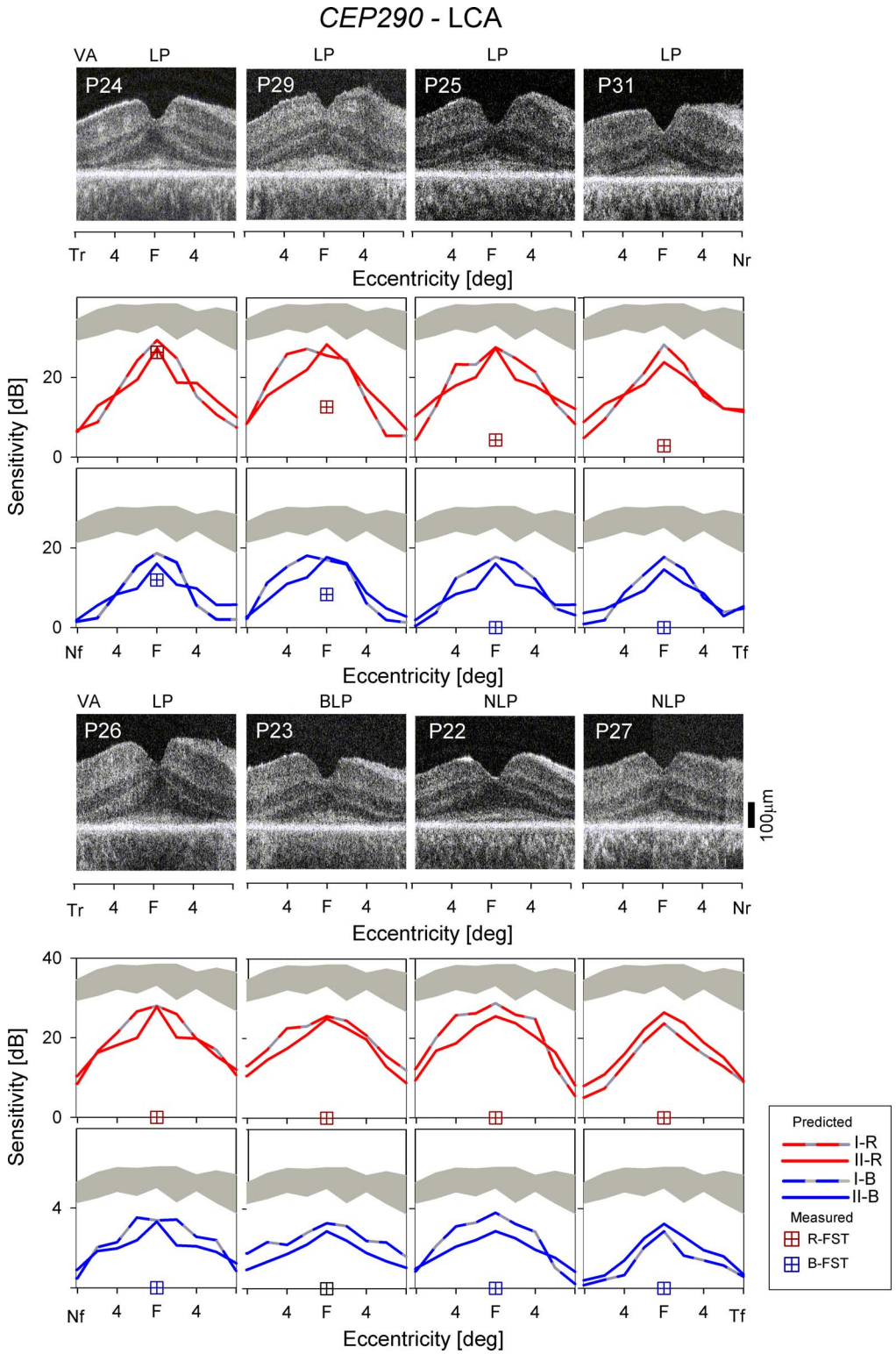

Figure 5. Predicted and measured sensitivities for *CEP290*-LCA patients with severe loss of visual acuity and fixation. The *upper row* shows OCT scans along the horizontal meridian across the fovea; visual acuities are given above the scans. *Middle row* plots measured R-FST sensitivities and predictions of Model I-R and Model II-R. *Lower row* compares the measured B-FST sensitivities with predictions of Models I-B and Model II-B. P24 had clinically LP vision but retained a log MAR of 2.6 with low-vision specific tests.

molecular diagnosis. Entry criteria tend to include certain ages and there are exclusions based on many considerations such as ocular and general health. Then, functional limits are set for inclusion (and exclusion) and, traditionally, the parameter that has been used is visual acuity.[59] Once a trial begins and safety outcomes are addressed, there is the inevitable question of whether there is any visual efficacy. If there is efficacy, it would be important to know the relationship of any positive visual

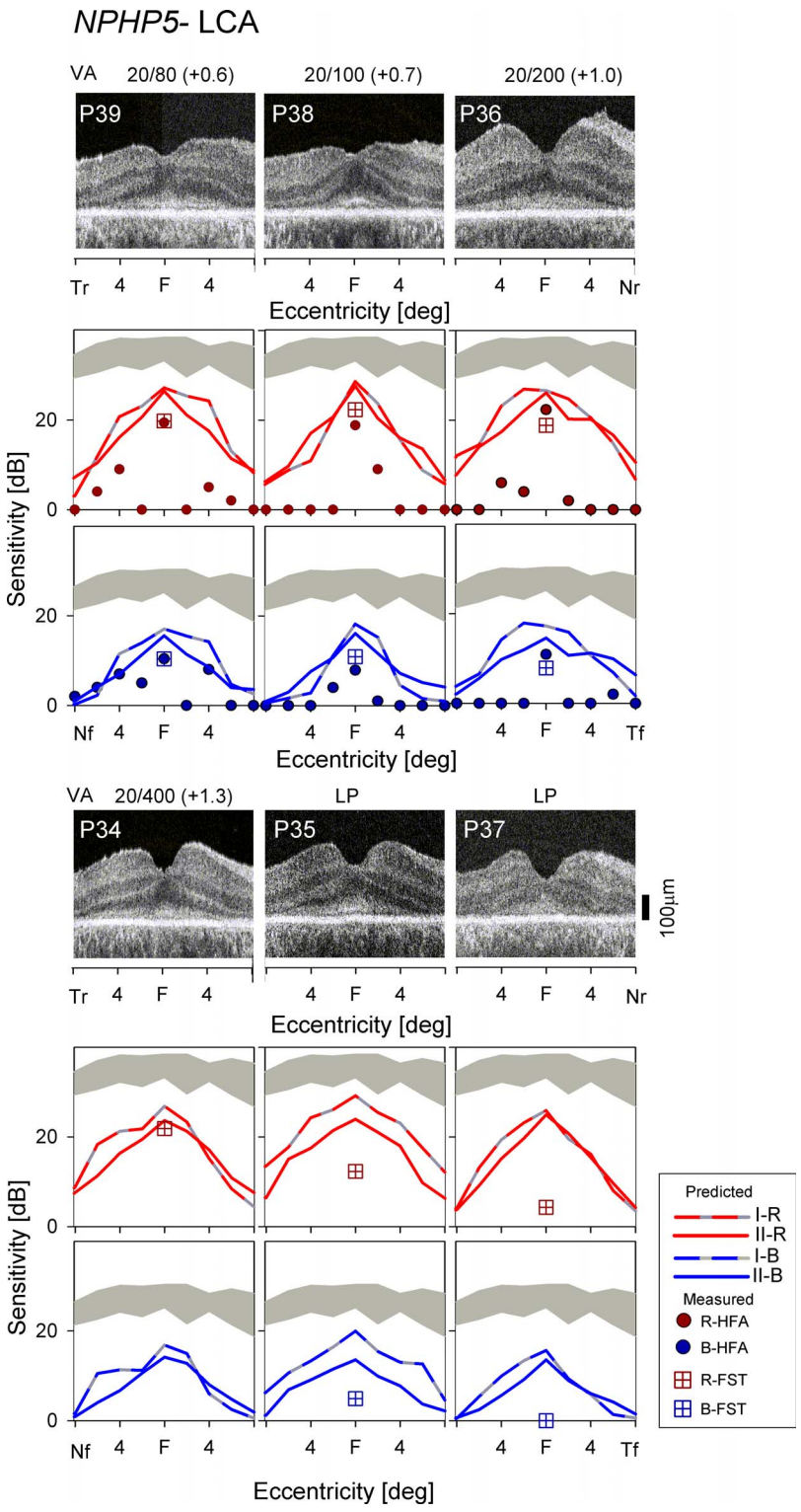

Figure 6. Predicted and measured sensitivities for *NPHP5*-LCA patients. *Upper row* shows OCT images of *NPHP5*-LCA patients; visual acuities are also given. *Middle row* plots measured R-HFA (*red circles*) or R-FST (*red boxes*) sensitivities alongside predicted sensitivities from Model I-R and Model II-R. *Lower panels* compare measured B-HFA (*blue circles*) or B-FST (*blue boxes*) with the predictions of Model I-B and Model II-B. Omitted B-FST sensitivity for P34 is due to mixed-mediation of this result; R-FST represents cone function but B-FST would represent rod function likely originating from the extrafoveal region.

change to what is expected for each patient, assuming an optimal treatment strategy. In the present era, however, we do not enter a clinical trial with an ability to make a quantitative prediction of outcome. In general, if acuity improves (to any degree) compared with baseline, success is announced, and the trial may move forward to later phases.

This is fully understandable. After the long history of no efficacious therapy for LCA, any improvement in vision is

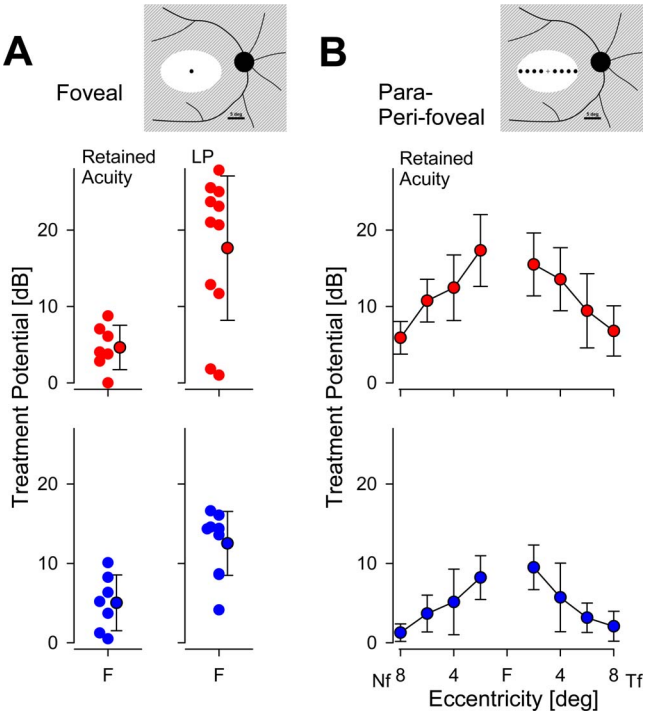

Figure 7. Treatment potential for *CEP290*- and *NPHP5*-LCA patients. (**A**) Foveal treatment potential with red (*upper*) and blue (*lower*) stimuli in the subset of patients with relatively retained acuity and fixation, and available perimetric testing (*left*). Also shown are the treatment potential in patients mostly with LP or worse vision and available FST sensitivity that is assumed to originate from the fovea (*right*). Data from individual patients are shown staggered to the *left* and mean ± SD of the groups are shown to the *right*. (**B**) Peri- and parafoveal treatment potential with red (*upper*) and blue (*lower*) stimuli in the subset of patients with relatively retained acuity and fixation, and available perimetric testing. *Insets* show the foveal and extra-foveal retinal locations tested on a retinal schematic, and the region that typically is outside of the central ellipse of retained ONL is *hashed* for reference.

welcomed by patients, investigators and trial sponsors alike. If the efficacy outcome is visual acuity and the change is deemed significant by some standard, questions are usually not asked about whether the positive effect is complete or partial. Indeed, why should visual acuity improve at all in non-regenerative therapies, such as gene augmentation or gene splice modulation, where new photoreceptor cells are not being introduced or regenerated? One of the likely possibilities for acuity improvement is a change in the perceived brightness of a spatial resolution target. It is long known that there is a strong relationship between acuity and perceived brightness in subjects with normal vision.[60] In retinal disease, brightness of the target depends on the light sensitivity of the retina at the locus of fixation in addition to the ambient lighting conditions. Strong correlative evidence of a relationship between acuity and light sensitivity existed in our cohort. *CEP290*- and *NPHP5*-LCA patients in this study had a spectrum of visual acuity results from 20/50 to NLP, consistent with previous reports.[61–64] Light sensitivity as measured with dark-adapted red (cone-mediated) FST measurements showed a relation with visual acuity – the better the visual acuity, the higher the FST sensitivities. To quantify this relation, patients were divided into the following two groups: group 1 had measurable acuities of 20/50 to 20/400 (logMAR 0.4–1.3) and an average FST of 24.3 dB; and group 2 had LP vision and an average FST of 6.9 dB. The FST measurements of these groups were statistically different (*t*-test, $P < 0.001$). Thus, we concentrated on light sensitivity as measured by FST in all subjects, or by perimetry in the subset of subjects with retained fixation, in order to describe the individual-specific treatment potential based on residual retinal structure. We assumed that sensitivity improvements are necessary for acuity improvements.

Treatment Potential With Optimal Efficacy

Not surprisingly, patients with the most severe losses of light sensitivity (but still retaining some photoreceptor structure) had the largest treatment potential. Extrapolating from the distribution of retinal function and structure in patients with relatively milder disease phenotype, we assume that the large treatment potential in severe patients localizes to the foveal area, which retains the most photoreceptors. The predictors for translating such a treatment potential in terms of light sensitivity into improved spatial vision (i.e., visual acuity) remain unknown at this time. It is likely that patients with congenital or very early onset loss of light sensitivity may be at a deep amblyopic disadvantage for gaining spatial vision as compared with others who may have had spatial vision in childhood that was lost in later years during disease progression.

Patients with relatively retained visual acuity, ability to fixate and small losses of light sensitivity had a relatively small treatment potential at the fovea. However, it is important to note that the treatment potential is estimated based on the retinal structure retained by each patient at the time of the intervention. If a treatment were to change the retinal structure in a positive direction, such as lengthening of the OS, the treatment potential at the fovea would also be expected to grow accordingly. Preliminary results in a recent clinical trial were suggestive that such positive structural changes in the outer retina are possible.[20]

Most unexpected was the parafoveal localization of a peak of treatment potential to an eccentricity of 2° in the patients with the relatively milder forms of *CEP290*- or *NPHP5*-LCA. There was relatively large treatment potential across the central macula. These results suggest that the expectation for efficacy in a clinical trial of these specific milder forms of LCA would not only be a small change in acuity and foveal sensitivity but also expansion of the central visual field by increases in cone visual sensitivity across the macular island. RP patients with a small central island of useful cone vision remaining can cope with the many demands on their daily lives.[65,66] Most *CEP290*- and *NPHP5*-LCA patients would be pleased to have a larger central island of vision with limits corresponding to their macular structure. If foveal improvement only was achieved after a certain therapeutic dosage, decisions could then be made about extending the length of the trial to determine if parafoveal loci responded later and whether further dosing should be considered. It is also important to consider that intravitreal and subretinal approaches to treatments may have different outcomes with respect to their foveal and extrafoveal effects.

Next Steps in This Research

Many inherited retinal diseases are in early phase clinical trials. Although the hope is that a therapy would cause a visual improvement, evidence for that assumption is lacking at present except for the LCA subtypes caused by *CEP290*, *NPHP5*, *GUCY2D*, and *RPE65* mutations. Artificial intelligence–based modeling as in the current work has not yet been used to analyze conditions with residual rod-mediated vision and structure. Gene based trials of rod photoreceptor diseases would benefit from such predictions. Accurate predictions of

therapeutic potential could move some retinal diseases from the category of interventions designed to slow progression to those designed to provide vision improvement.

Acknowledgments

Supported by grants from the National Institutes of Health (R01-EY017549; P30-EY001583; Bethesda, MD, USA), ProQR Therapeutics (Leiden, the Netherlands), The Chatlos Foundation (Longwood, FL, USA), and Research to Prevent Blindness (New York, NY, USA).

Disclosure: **A. Sumaroka**, None; **A.V. Garafalo**, None; **E.P. Semenov**, None; **R. Sheplock**, None; **A.K. Krishnan**, None; **A.J. Roman**, None; **S.G. Jacobson**, ProQR (F), P; **A.V. Cideciyan**, ProQR (F), P

References

1. Recommendations on Clinical Assessment of Patients with Inherited Retinal Degenerations - 2016. American Academy of Ophthalmology Clinical Education/Guidelines/Clinical Statements; 2016. Available at: https://www.aao.org/clinical-statement/recommendations-on-clinical-assessment-of patients. Accessed February 27, 2019.
2. Duncan JL, Pierce EA, Laster AM, et al. Inherited retinal degenerations: current landscape and knowledge gaps. *Trans Vis Sci Tech*. 2018;7(4):6.
3. Marmor MF, Aguirre G, Arden G, et al. Retinitis pigmentosa: a symposium on terminology and methods of examination. *Ophthalmology*. 1983;90:126–131.
4. Jacobson SG, Cideciyan AV, Roman AJ, et al. Improvement and decline in vision with gene therapy in childhood blindness. *N Engl J Med*. 2015;372:1920–1926.
5. Bainbridge JW, Mehat MS, Dundaram V, et al. Long-term effects of gene therapy on Leber's congenital amaurosis. *N Engl J Med*. 2015;372:1887–1897.
6. Jacobson SG, Aleman TS, Cideciyan AV, et al. Identifying photoreceptors in blind eyes caused by RPE65 mutations: prerequisite for human gene therapy success. *Proc Natl Acad Sci U S A*. 2005;102:6177–6182.
7. Acland GM, Aguirre GD, Ray J, et al. Gene therapy restores vision in a canine model of childhood blindness. *Nat Genet*. 2001;28:92–95.
8. Pang JJ, Chang B, Kumar A, et al. Gene therapy restores vision-dependent behavior as well as retinal structure and function in a mouse model of RPE65 Leber congenital amaurosis. *Mol Ther*. 2006;13:565–572.
9. Cideciyan AV. Leber congenital amaurosis due to RPE65 mutations and its treatment with gene therapy. *Prog Retin Eye Res*. 2010;29:398–427.
10. Chang B, Khanna H, Hawes N, et al. In-frame deletion in a novel centrosomal/ciliary protein CEP290/NPHP6 perturbs its interaction with RPGR and results in early-onset retinal degeneration in the rd16 mouse. *Hum Mol Genet*. 2006;15:1847–1857.
11. Schäfer T, Pütz M, Lienkamp S, et al. Genetic and physical interaction between the NPHP5 and NPHP6 gene products. *Hum Mol Genet*. 2008;17:3655–3662.
12. Barbelanne M, Song J, Ahmadzai M, Tsang WY. Pathogenic NPHP5 mutations impair protein interaction with Cep290, a prerequisite for ciliogenesis. *Hum Mol Genet*. 2013;22:2482–2494.
13. Takao D, Wang L, Boss A, Verhey KJ. Protein interaction analysis provides a map of the spatial and temporal organization of the ciliary gating zone. *Curr Biol*. 2017;27:2296–2306.
14. Cideciyan AV, Aleman TS, Jacobson SG, et al. Centrosomal-ciliary gene CEP290/NPHP6 mutations result in blindness with unexpected sparing of photoreceptors and visual brain: implications for therapy of Leber congenital amaurosis. *Hum Mutat*. 2007;28:1074–1083.
15. Cideciyan AV, Rachel RA, Aleman TS, et al. Cone photoreceptors are the main targets for gene therapy of NPHP5 (IQCB1) or NPHP6 (CEP290) blindness: generation of an all-cone Nphp6 hypomorph mouse that mimics the human retinal ciliopathy. *Hum Mol Genet*. 2011;20:1411–1423.
16. Stone EM, Cideciyan AV, Aleman TS, et al. Variations in NPHP5 in patients with nonsyndromic Leber congenital amaurosis and Senior-Loken syndrome. *Arch Ophthalmol*. 2011;129:81–87.
17. Estrada-Cuzcano A, Koenekoop RK, Coppieters F, et al. IQCB1 mutations in patients with Leber congenital amaurosis. *Invest Ophthalmol Vis Sci*. 2011;52:834–839.
18. Downs LM, Scott EM, Cideciyan AV, et al. Overlap of abnormal photoreceptor development and progressive degeneration in Leber congenital amaurosis caused by NPHP5 mutation. *Hum Mol Genet*. 2016;25:4211–4226.
19. Jacobson SG, Cideciyan AV, Sumaroka A, et al. Outcome measures for clinical trials of Leber congenital amaurosis caused by the intronic mutation in the CEP290 gene. *Invest Ophthalmol Vis Sci*. 2017;58:2609–2622.
20. Cideciyan AV, Jacobson SG, Drack AV, et al. Effect of an intravitreal antisense oligonucleotide on vision in Leber congenital amaurosis due to a photoreceptor cilium defect. *Nat Med*. 2019;25:225–228.
21. Maeder ML, Stefanidakis M, Wilson CJ, et al. Development of a gene-editing approach to restore vision loss in Leber congenital amaurosis type 10. *Nat Med*. 2019;25:229–233.
22. Caixinha M, Nunes S. Machine learning techniques in clinical vision sciences. *Curr Eye Res*. 2017;42:1–15.
23. Lu W, Tong Y, Yu Y, Xing Y, Chen C, Shen Y. Applications of artificial intelligence in ophthalmology: general overview. *J Ophthalmol*. 2018;2018:5278196.
24. Schmidt-Erfurth U, Sadeghipour A, Gerendas BS, Waldstein SM, Bogunović H. Artificial intelligence in retina. *Prog Retin Eye Res*. 2018;67:1–29.
25. Jacobson SG, Roman AJ, Aleman TS, et al. Normal central retinal function and structure preserved in retinitis pigmentosa. *Invest Ophthalmol Vis Sci*. 2010;51:1079–1085.
26. Sumaroka A, Matsui R, Cideciyan AV, et al. Outer retinal changes including the ellipsoid zone band in Usher syndrome 1B due to MYO7A mutations. *Invest Ophthalmol Vis Sci*. 2016;57:OCT253–OCT261.
27. Sumaroka A, Garafalo AV, Cideciyan AV, et al. Blue cone monochromacy caused by the C203R missense mutation or large deletion mutations. *Invest Ophthalmol Vis Sci*. 2018;59:5762–5772.
28. Sadigh S, Luo X, Cideciyan AV, et al. Drusen and photoreceptor abnormalities in African-Americans with intermediate non-neovascular age-related macular degeneration. *Curr Eye Res*. 2015;40:398–406.
29. Jacobson SG, Voigt WJ, Parel JM, et al. Automated light- and dark-adapted perimetry for evaluating retinitis pigmentosa. *Ophthalmology*. 1986;93:1604–1611.
30. Roman AJ, Schwartz SB, Aleman TS, et al. Quantifying rod photoreceptor-mediated vision in retinal degenerations: dark-adapted thresholds as outcome measures. *Exp Eye Res*. 2005;80:259–272.
31. Roman AJ, Cideciyan AV, Aleman TS, Jacobson SG. Full-field stimulus testing (FST) to quantify visual perception in severely blind candidates for treatment trials. *Physiol Meas*. 2007;28:N51–N56.
32. Breiman L. Random forests. *Machine Learning*. 2001;45:5–32.

Investigative Ophthalmology & Visual Science

33. Bland JM, Altman DG. Measuring agreement in method comparison studies. *Stat Methods Med Res*. 1999;8:135–160.
34. Boye SE, Huang WC, Roman AJ, et al. Natural history of cone disease in the murine model of Leber congenital amaurosis due to CEP290 mutation: determining the timing and expectation of therapy. *PLoS One*. 2014;9:e92928.
35. Jacobson SG, Cideciyan AV, Huang WC, et al. Leber congenital amaurosis: genotypes and retinal structure phenotypes. *Adv Exp Med Biol*. 2016;854:169–175.
36. Cideciyan AV, Jacobson SG. Leber congenital amaurosis (LCA): potential for improvement of vision – The Proctor Lecture. *Invest Ophthalmol Vis Sci*. 2019;60:1680–1695.
37. Bramall AN, Wright AF, Jacobson SG, McInnes RR. The genomic, biochemical, and cellular responses of the retina in inherited photoreceptor degenerations and prospects for the treatment of these disorders. *Annu Rev Neurosci*. 2010; 33:441–472.
38. Wright AF, Chakarova CF, Abd El-Aziz MM, Bhattacharya SS. Photoreceptor degeneration: genetic and mechanistic dissection of a complex trait. *Nat Rev Genet*. 2010;11:273–284.
39. Verbakel SK, van Huet RAC, Boon CJF, et al. Non-syndromic retinitis pigmentosa. *Prog Retin Eye Res*. 2018;66:157–186.
40. Calzetti G, Levy RA, Cideciyan AV, et al. Efficacy outcome measures for clinical trials of USH2A caused by the common c.2299delG mutation. *Am J Ophthalmol*. 2018;193:114–129.
41. Cideciyan AV, Charng J, Roman AJ, et al. Progression in X-linked retinitis pigmentosa due to ORF15-RPGR mutations: assessment of localized vision changes over 2 years. *Invest Ophthalmol Vis Sci*. 2018;59:4558–4566.
42. Huang Y, Cideciyan AV, Papastergiou GI, et al. Relation of optical coherence tomography to microanatomy in normal and rd chickens. *Invest Ophthalmol Vis Sci*. 1998;39:2405–2416.
43. Spaide RF, Curcio CA. Anatomical correlates to the bands seen in the outer retina by optical coherence tomography: literature review and model. *Retina*. 2011;31:1609–1619.
44. Jonnal RS, Kocaoglu OP, Zawadzki RJ, et al. The cellular origins of the outer retinal bands in optical coherence tomography images. *Invest Ophthalmol Vis Sci*. 2014; 16; 55:7904–7918.
45. Rangaswamy NV, Patel HM, Locke KG, Hood DC, Birch DG. A comparison of visual field sensitivity to photoreceptor thickness in retinitis pigmentosa. *Invest Ophthalmol Vis Sci*. 2010;51:4213–4219.
46. Sayo A, Ueno S, Kominami T, et al. Significant relationship of visual field sensitivity in central 10° to thickness of retinal layers in retinitis pigmentosa. *Invest Ophthalmol Vis Sci*. 2018;59:3469–3475.
47. Jacobson SG, Cideciyan AV, Aleman TS, et al. RDH12 and RPE65, visual cycle genes causing Leber congenital amaurosis, differ in disease expression. *Invest Ophthalmol Vis Sci*. 2007; 48:332–338.
48. Jacobson SG, Cideciyan AV, Huang WC, et al. TULP1 mutations causing early-onset retinal degeneration: preserved but insensitive macular cones. *Invest Ophthalmol Vis Sci*. 2014;55:5354–5364.
49. Esteva A, Robicquet A, Ramsundar B, et al. A guide to deep learning in healthcare. *Nat Med*. 2019;25:24–29.
50. Lee CS, Baughman DM, Lee AY. Deep neural learning is effective for classifying normal versus age-related macular degeneration in OCT images. *Ophthalmol Retina*. 2017;1: 322–327.
51. Muhammad H, Fuchs TJ, De Cuir N, et al. Hybrid deep learning on single wide-field optical coherence tomography scans accurately classifies glaucoma suspects. *J Glaucoma*. 2017;26:1086–1094.
52. Hussain MA, Bhuiyan A, Luu CD, et al. Classification of healthy and diseased retina using SD-OCT imaging and random forest algorithm. *PLoS One*. 2018;13:e0198281.
53. Kermany DS, Goldbaum M, Cai W, et al. Identifying medical diagnoses and treatable diseases by image-based deep learning. *Cell*. 2018;172:1122–1131.
54. Fang L, Cunefare D, Wang C, et al. Automatic segmentation of nine retinal layer boundaries in OCT images of non-exudative AMD patients using deep learning and graph search. *Biomed Opt Express*. 2017;8:2732–2744.
55. Kugelman J, Alonso-Caneiro D, Read SA, Vincent SJ, Collins MJ. Automatic segmentation of OCT retinal boundaries using recurrent neural networks and graph search. *Biomed Opt Express*. 2018; 2018;9:5759–5777.
56. Schmidt-Elfurth U, Bogunovid H, Sadeghipour A, et al. Machine learning to analyze the prognostic value of current imaging biomarkers in neovascular age-related macular degeneration. *Opthalmol Retina*. 2018;2:24–30.
57. Wen JC, Lee CS, Keane PA, et al. Forecasting future Humphrey visual fields using deep learning. *PLoS One*. 2019;14: e0214875.
58. Kihara Y, Heeren TFC, Lee CS, et al. Estimating retinal sensitivity using optical coherence tomography with deep-learning algorithms in macular telangiectasia type 2. *JAMA Netw Open*. 2019;2:e188029.
59. Beck RW, Maguire MG, Bressler NM, et al. Visual acuity as an outcome measure in clinical trials of retinal diseases. *Ophthalmology*. 2007;114:1804–1809.
60. Berger C. The dependency of visual acuity on illumination and its relation to the size and function of the retinal units. *Am J Psychol*. 1941;54:336–352.
61. Walia S, Fishman GA, Jacobson SG, et al. Visual acuity in patients with Leber's congenital amaurosis and early childhood-onset retinitis pigmentosa. *Ophthalmology*. 2010;117: 1190–1198.
62. McAnany JJ, Genead MA, Walia S, et al. Visual acuity changes in patients with leber congenital amaurosis and mutations in CEP290. *JAMA Ophthalmol*. 2013;131:178–182.
63. Sheck L, Davies WIL, Moradi P, et al. Leber congenital amaurosis associated with mutations in CEP290, clinical phenotype, and natural history in preparation for trials of novel therapies. *Ophthalmology*. 2018;125:894–903.
64. Valkenburg D, van Cauwenbergh C, Lorenz B, et al. Clinical characterization of 66 patients with congenital retinal disease due to the deep-intronic c.2991+1655A>G mutation in CEP290. *Invest Ophthalmol Vis Sci*. 2018;59:4384–4391.
65. Szlyk JP, Fishman GA, Alexander KR, et al. Relationship between difficulty in performing daily activities and clinical measures of visual function in patients with retinitis pigmentosa. *Arch Ophthalmol*. 1997;115:53–59.
66. Turano KA, Geruschat DR, Stahl JW, Massof RW. Perceived visual ability for independent mobility in persons with retinitis pigmentosa. *Invest Ophthalmol Vis Sci*. 1999;40: 865–877.

Investigative Ophthalmology & Visual Science